



HHS Public Access

Author manuscript

Nat Struct Mol Biol. Author manuscript; available in PMC 2013 November 01.

Published in final edited form as:

Nat Struct Mol Biol. 2013 May ; 20(5): 634–640. doi:10.1038/nsmb.2548.

Binding thermodynamics of a glutamate transporter homologue

Nicolas Reyes^{1,2}, SeCheol Oh¹, and Olga Boudker¹

¹Department of Physiology and Biophysics, Weill Cornell Medical College, New York, New York, USA

Abstract

Glutamate transporters catalyze concentrative uptake of the neurotransmitter into glial cells and neurons. Their transport cycle involves binding and release of the substrate on the extra- and intracellular sides of the plasma membranes, and translocation of the substrate-binding site across the lipid bilayers. The energy of the ionic gradients, mainly sodium, fuels the cycle. Here, we used a cross-linking approach to trap a glutamate transporter homologue from *Pyrococcus horikoshii* in key conformational states with substrate-binding site facing either the extracellular or intracellular sides of the membrane to study their binding thermodynamics. We show that the chemical potential of sodium ions in solution is exclusively coupled to substrate binding and release, and not to substrate translocation. Despite the structural symmetry, the binding mechanisms are distinct on the opposite sides of the membrane and more complex than the current models suggest.

Introduction

Ion-coupled active transporters move their substrates against concentration gradients using the energy of ionic gradients. To achieve this, the coupled ions drive cycles of conformational changes, which entail the transporter binding its substrate on one side of the membrane, translocating and releasing it on the other side, and finally returning to the initial conformation (Fig. 1a). Despite the wealth of the functional and structural data supporting this view, the role of ions in this process remains incompletely understood, and several mechanisms of coupling have been proposed¹. Some of them suggest that the ions control the substrate binding affinity on the opposite sides of the membrane, while others focus on their role in modulating the kinetics of the translocation steps^{1,2}.

The paucity of the confirmed coupling mechanisms is largely due to the experimental challenges of dissecting the role of ions in substrate binding and in translocation reactions. To circumvent these difficulties and to probe the role of ions in the isolated steps of a transport cycle, we have developed a novel experimental approach, using a prokaryotic homologue of the glutamate transporter family, Glt_{Ph}, as a model system. Glt_{Ph} originates

Users may view, print, copy, download and text and data- mine the content in such documents, for the purposes of academic research, subject always to the full Conditions of use: http://www.nature.com/authors/editorial_policies/license.html#terms

Correspondence should be addressed to: OB, olb2003@med.cornell.edu; and NR, nicolas.reyes@pasteur.fr.

²Current address: Molecular Mechanisms of Membrane Transport Unit (CNRS UMR 3528), Department of Structural Biology and Chemistry, Institut Pasteur, Paris, France

Author contributions N.R. and O.B. designed the experiments. N.R. and S.O. conducted the experiments, and N.R. and O.B. analyzed the data and wrote the manuscript.

from a hyper-thermophilic archaeon *Pyrococcus horikoshii*, and symports aspartate and sodium with a 1:3 substrate to ion stoichiometry^{3,4}. It is the only member of the family with known high-resolution structures^{5–8}. The crystallographic studies have shown that the translocation of the substrate-binding site across the membrane involves a 15–18 Å trans-membrane movement of a peripheral transport domain relative to a central trimerization domain (Fig. 1b)^{5–8}. The latter mediates the inter-subunit contacts within the trimeric Glt_{Ph}, while the former coordinates sodium (Na⁺) ions and substrate L-aspartate (Asp). The Asp and two Na⁺ binding sites have been identified crystallographically; the location of the third Na⁺ site is still debated^{6,9–15}. Na1 site is located deep in the core of the transport domain, while Na2 site is on the surface and is formed in part by the helical hairpin (HP) 2 (Fig.1b). Notably, bound Asp does not contribute directly to either of the sites. The structures of the unbound transporter and hence, the mechanisms by which the substrate and ions are released remain unknown. However, a clue is provided by a structure of Glt_{Ph} in the outward facing state in complex with a competitive blocker, L-threo-β-benzyloxyaspartate (L-TBOA)⁶, in which the blocker is bound in the substrate-binding pocket with its benzyl group propping HP2 in an open conformation and disrupting Na2 binding site, suggesting that HP2 serves as the extracellular gate of the transporter^{6,16–18}.

To dissect the mechanism of the energetic coupling between binding of Na⁺ ions and Asp to the isolated outward and inward facing states of Glt_{Ph}, we introduced pairs of cysteine mutations, one in the transport domain and the other in the trimerization domain, which upon cross-linking trapped the transporter in either of these states and disallowed the translocation steps (Fig. 1b). Using this approach, we show that in both the outward and inward facing states binding of Asp is coupled to binding of all 3 co-transported Na⁺ ions and that binding of the ligands is highly cooperative. Hence, essentially all available chemical potential of Na⁺ ions is coupled to substrate binding, while further conformational changes, including the trans-membrane movements of the transport domains, occur independently of the ions. Furthermore, based on the experimentally determined heat capacity changes upon binding, we conclude that despite similar structure of the substrate and ion binding sites in the outward and inward facing states, the molecular events underlying binding, particularly of the first 2 Na⁺ ions, are distinct in these states and are more complex than available crystal structures would suggest.

Results

Trapping Glt_{Ph} in the outward and inward facing states

To characterize the binding properties of the main conformational states of Glt_{Ph}, we “stapled” together the transport and trimerization domains in either the outward or inward facing states using mercury (Hg²⁺)-mediated cross-linking of double cysteine mutants. Previous studies showed that in Hg²⁺-crosslinked Glt_{Ph} K55C A364C (Glt_{Ph}ⁱⁿ), the transport domain is trapped in the inward-facing position⁷. By analogy, we engineered a double cysteine mutant Glt_{Ph} L66C S300C based on the outward facing structure of the wild type (WT) Glt_{Ph}⁶. Following crosslinking, we confirmed the outward orientation of the transport domain by crystallography (Glt_{Ph}^{out}, Fig. 1b, Table 1, Supplementary Fig. 1). Like Glt_{Ph}ⁱⁿ, Glt_{Ph}^{out} shows peaks in the anomalous difference Fourier maps adjacent to the sulfur atoms

of the cysteine residues (Supplementary Fig. 1b), revealing Hg^{2+} ions in the expected positions and distant from the substrate and ion binding sites (Fig. 1b). Structures of $\text{Glt}_{\text{Ph}}^{\text{out}}$ and $\text{Glt}_{\text{Ph}}^{\text{in}}$ (ref. 5 and this study) were similar to those obtained in the absence of cross-links^{6,8} (with root mean squared deviations of ~ 0.9 Å). Isothermal titration calorimetry (ITC) experiments showed that Hg^{2+} binds to the Glt_{Ph} L66C S300C and Glt_{Ph} K55C A364C protomers with 1:1 stoichiometry and nanomolar affinity both in the substrate bound and free states (Fig. 1c and Supplementary Table 1). These results confirm that Hg^{2+} -crosslinking traps the mutant transporters in the outward and inward facing states, respectively, regardless of whether they are bound to the substrate or not.

Ions drive substrate binding to the isolated states

Using ITC, we showed that Asp binds with 1:1 stoichiometry and similar affinities to $\text{Glt}_{\text{Ph}}^{\text{out}}$, $\text{Glt}_{\text{Ph}}^{\text{in}}$ and the unconstrained WT transporter in the presence of 10 mM Na^+ (Fig. 2a). The dissociation constants (K_{DS}) were 240 ± 50 , 290 ± 30 and 480 ± 10 nM, respectively. Hence, the transporter has similar intrinsic affinities for its substrate on the opposite sides of the membrane at 25 °C. Similar results have been obtained in other families of ion-coupled transporters².

Binding of Asp to WT Glt_{Ph} was shown to be coupled to binding of Na^+ ions⁶. We asked whether this coupling is a property intrinsic to the outward and inward facing states or whether it requires unrestrained movements of the transport domain. To explore a wide range of binding constants, we optimized a fluorescence-based assay, developed by the Apell laboratory^{19,20}. A voltage sensitive amphipathic dye, RH421, is incorporated into the protein/detergent particles and reports on binding of ligands that alter the local electric field²¹. Coupled Na^+ and Asp binding was measured by detecting the decrease in the emission intensity of the probe (Fig. 2b, Supplementary Fig. 2a). The K_{DS} , obtained by fitting the normalized fluorescence changes, were in excellent agreement with those obtained in ITC experiments (Fig. 2c).

The Asp K_{DS} of all transporter variants were strongly Na^+ -dependent, and the logarithmic plots of the affinities as a function of Na^+ activity yielded straight lines with slopes of 2.6, 2.6 and 2.9 for $\text{Glt}_{\text{Ph}}^{\text{out}}$, $\text{Glt}_{\text{Ph}}^{\text{in}}$ and WT, respectively. These slopes represent the apparent numbers of Na^+ ions coupled to binding of each substrate molecule. Hence, Asp binding is thermodynamically linked to binding of all three transported Na^+ ions in WT Glt_{Ph} . Moreover, in the constrained mutants the coupling efficiencies are similar, showing that transport domain movements are not necessary. We conclude that essentially all chemical potential of Na^+ ions is transformed into substrate binding energy. These results contrast with the coupling mechanisms proposed for other families of secondary active transporters, in which the coupled ions do not change the affinity for the substrate² or the substrate can bind in the absence of coupled ions²².

Functional studies on the mammalian glutamate transporters showed that, like in Glt_{Ph} , 3 Na^+ ions are co-transported with each substrate^{23–25}. Because of the high degree of conservation of residues involved in Na^+ and substrate coordination between Glt_{Ph} and the mammalian homologues, it is likely that the efficient coupling between substrate and ions is also conserved. However, glutamate K_m decreases approximately linearly with the increase

of Na^+ concentration^{12,26}, corresponding to the slope of ~ 1 on the logarithmic plot. The relative insensitivity of the glutamate K_m values to Na^+ concentrations likely reflects the significant contributions from other steps in the cycle following binding, in particular the dissociation of the substrate on the opposite side of the membrane.

Inhibitor captures early events of the binding reaction

In parallel, we examined binding of inhibitors, L-threo- β -benzylaspartate (TBA)²⁷, and DL-TBOA²⁸. In these experiments, we focused on TBA rather than on the commonly used and structurally similar DL-TBOA because the latter is a mixture of stereoisomers, binding to the transporters with different affinities²⁹ and complicating the analysis. TBA inhibits Asp transport by Glt_{Ph} (Supplementary Fig. 2b) and binds to the constrained variants and WT Glt_{Ph} with similar affinities (Fig. 2c). The Na^+ dependence of TBA binding affinity was also similar for $\text{Glt}_{\text{Ph}}^{\text{out}}$, $\text{Glt}_{\text{Ph}}^{\text{in}}$ and WT, and was weaker than that for Asp with slopes of 1.9, 2.2, and 1.6, respectively (Fig. 2c).

To confirm that TBA binds to the same site as Asp, we first saturated the transporters with TBA and then titrated them with Asp using ITC. As expected for the competitive binding, the free energies and enthalpies of Asp binding to TBA-loaded transporters agree with the values calculated for TBA replacement by Asp using the individually measured binding parameters (Supplementary Fig. 3, Supplementary Table 1). We conclude that TBA binds to both the outward and inward facing states in the substrate binding pockets, disrupting one of the Na^+ binding sites. These results are in excellent agreement with previous studies, showing that L-TBOA binds to the outward facing Glt_{Ph} with its backbone in the substrate binding site and the benzyl group preventing HP2 from occluding the site and forming Na2 site⁶. Based on this, we hypothesize that the TBA-bound states can be viewed as intermediates of the binding reactions, in which two Na^+ ions and Asp are already bound but not yet occluded. If so, TBA offers a tool to gain insights into the energetics of the two processes: the initial binding of the substrate coupled to two Na^+ ions, and its occlusion coupled to the third Na^+ ion. The latter process is represented by the TBA replacement with Asp.

Na^+ binding and allosteric coupling

Using the fluorescence-based assay, we also examined Na^+ binding to Glt_{Ph} variants in the absence of Asp and TBA. Na^+ binds weakly to the WT and constrained transporters with K_D s above 50 mM, corresponding to the binding free energy of approximately -1 kcal mol^{-1} (Fig. 3). In the case of $\text{Glt}_{\text{Ph}}^{\text{in}}$, we were unable to reach saturation due to nonspecific effects of Na^+ concentrations above 500 mM on the fluorescent probe. In this case, the estimation of $\text{Na}^+ K_D$ was not significantly affected, but an accurate determination of the Hill coefficient was not possible. In contrast, both $\text{Glt}_{\text{Ph}}^{\text{out}}$ and WT transporter yielded reproducible Hill coefficients of 1.6, suggesting that the transporters bind at least 2 sodium ions in the absence of other ligands. Because the architecture of Na^+ binding sites is similar in the inward and outward facing states, we tentatively conclude that 2 Na^+ ions bind to both states. Additions of Asp and TBA shift the Na^+ binding isotherms to lower concentrations in all cases as expected for cooperative binding (Fig. 3 and Supplementary Fig. 4). The ability of the transporter to bind Na^+ in the absence of substrate may account for a previously

reported weaker coupling between binding of Asp and Na⁺ ions to the WT Glt_{Ph}⁶. In this earlier study, measurements of Asp binding in the presence of Na⁺ concentrations of up to 200 mM have been included; under these conditions some of the sodium ion binding sites are already occupied.

To evaluate the standard free energies, G^0 , of the coupled binding of 3 Na⁺ and Asp or 2 Na⁺ and TBA, we note that the observed free energy, G_{app} can be expressed as:

$$\Delta G_{app} = \Delta G^0 - \alpha \times \mu_{Na} \quad (1)$$

where μ_{Na} is the chemical potential of Na⁺ ions and α is the apparent number of Na⁺ ions coupled to binding of the ligand (Supplementary Note). From the linear fits in Fig. 2c, we obtain G^0 of 3 Na⁺ and Asp and 2 Na⁺ and TBA binding to Glt_{Ph} of ~ -16 and ~ -10 kcal mol⁻¹, respectively, for both the outward and inward facing states. Importantly, only small fractions of these large favorable free energies originate from binding of Na⁺ ions, inhibitor or substrate alone, and the majority comes from coupling between the ligands. To the extent of our current knowledge, the substrate does not directly coordinate Na⁺ ions, and the observed cooperativity must arise from allosteric interactions.

The thermodynamic mechanisms

The magnitude of the heat capacity changes upon binding, C_p , is a unique experimental readout of the complexity of the underlying reaction, which can often be related to the extent of the protein conformational changes^{30–33}. Hence, we determined C_p s associated with overall binding of 3 Na⁺ and Asp and key intermediate steps: binding of the first 2 Na⁺ ions, binding of TBA, mimicking initial substrate binding, and TBA displacement by Asp, mimicking substrate occlusion and binding of the third Na⁺ ion.

To obtain C_p of the overall reaction, we determined the temperature dependence of the enthalpy (H) of Asp binding in the presence of Na⁺ concentrations below 50 mM. Under these conditions, there is little ion binding alone, and only the coupled binding of 3 Na⁺ and Asp is observed. The reaction H decreased linearly with temperature, yielding very large negative C_p s, constant within the tested temperature range (Fig. 4). Unexpectedly, we found that C_p s were significantly larger in the inward (-600 cal mol⁻¹ K⁻¹) compared to the outward facing state (-300 cal mol⁻¹ K⁻¹). This is in a sharp contrast with the structures, picturing nearly identical ion- and substrate-binding sites, and with the similar observed K_D s at 25 °C. In reactions dominated by protein conformational changes, C_p scales linearly with the buried polar and apolar surface areas³¹. If so, the observed C_p s would require burial of ~ 2000 and ~ 4000 Å² of the protein surface in the outward and inward facing states, respectively³¹. The current models suggest that the release of the substrate from the outward and inward facing states is associated with the openings of the local gates: HP2 in the former and a structurally symmetric HP1 in the latter^{6,7,16–18,34}. However, we estimate that HP2 closure buries only ~ 200 Å², expected to give C_p of approximately -30 cal mol⁻¹ K⁻¹. In fact, the experimental C_p s are so large that they cannot be explained by protein conformational changes alone. Previously, unexpectedly large C_p s have been attributed to the entrapment of structured waters in the protein core during binding³⁵, to heterogeneous apo state³⁶ and to protein rigidification³⁷ or folding coupled to binding³⁸. Although we

cannot distinguish between these possibilities, it is clear that binding involves more complex events in addition to the local conformational changes, and that these events are more extensive in the inward facing state.

Na⁺ binds too weakly to be measured by ITC directly. Instead, we measured H and C_P of Asp binding to Glt_{Ph}^{out} and Glt_{Ph}ⁱⁿ in the presence of 1 M Na⁺ (Fig. 4). Under these conditions all sites, to which Na⁺ ions bind in the absence of Asp, are occupied (Fig. 3). We observed that Asp binds to Na⁺-saturated transporter with 1:1 stoichiometry and K_{DS} in the nM range or lower (Supplementary Fig. 5A). To obtain C_{Ps} of Na⁺ binding, we calculated the differences between C_{Ps} of Asp binding in the presence and in the absence of 1 M Na⁺ (Supplementary Note and Supplementary Fig. 5B). From this analysis, we found that binding of Na⁺ ions alone is already associated with large negative C_{Ps} and that the differences between the C_{Ps} of the coupled binding of 3 Na⁺ and Asp in the outward and inward facing states are almost entirely due to the differences in ion binding.

The H and C_P values of TBA displacement by Asp were measured directly (Supplementary Fig. 3b). The C_{Ps} of TBA binding to Na⁺-saturated transporter were then calculated as differences between the corresponding values for Asp binding in 1 M Na⁺ and TBA displacement (Supplementary Note and Supplementary Fig. 5B). From these calculations, the C_{Ps} of TBA binding to Na⁺-saturated transporter were close to 0 in the outward and inward facing states (Fig. 5). As expected, similar small C_{Ps} were calculated for D,L-TBOA (Supplementary Fig. 6). These measurements suggest that binding of the substrate backbone, mimicked by the inhibitor, occurs with little C_P as is typical for a small molecule binding to a pre-formed site³⁹. The C_P values of Asp replacement of TBA, which mimics substrate occlusion and binding of the last Na⁺, were also similar in the outward and inward facing states (Fig 5). Notably, TBA is not likely to bind similarly in the two states: in the outward facing transport domain, the benzyl group is expected to prop HP2 in an open state, a conformation, which would be sterically prohibited when the domain is facing inward. Interestingly, the C_{Ps} were again significantly larger than expected for HP2 closure, suggesting that during these steps of the binding reactions, events other than gate closures dominate the processes.

Extrapolations to physiological temperatures

Our experiments were conducted at 25 °C, below the physiologic temperatures of ~100 °C, at which Glt_{Ph} normally operates. At 25 °C, Glt_{Ph} has a very high affinity for Asp making it an inefficient enzyme. Because the affinity is strongly dependent on Na⁺ concentration the transporter is functional, albeit slow, when reconstituted into proteo-liposomes with the internal Na⁺ near 0^{3,6}. In contrast, Glt_{Ph} should be largely inactive when expressed in mesophilic cells: considering the intracellular concentrations of Na⁺ and Asp on the order of 10 and 1 mM, respectively, only 0.05 % of the inward facing transporters will be substrate-free, rendering them highly inefficient.

Many enzymes from thermophilic organisms are either completely inactive or very slow at ambient temperatures⁴⁰, but when assayed at their physiological temperatures closely mimic their mesophilic counterparts⁴¹. To extrapolated the binding free energies to 100 °C, we used the standard thermodynamic equation:

$$\Delta G = \Delta G_{ref} + \Delta C_p (T - T_{ref}) - T \Delta C_p \ln \left(\frac{T}{T_{ref}} \right) \quad (2)$$

where G_{ref} is the free energy change measured at $T_{ref} = 25$ °C (Supplementary Note). Such extrapolation is valid when C_p does not change significantly with temperature. It is possible that this assumption does not hold and hence, the obtained values reflect the general trend rather than precise estimates. Because the heat capacities differ significantly in the outward and inward facing state, the Asp affinities diverge at higher temperatures and are estimated to be 6.3 and 1400 μM , respectively, at 100 mM Na^+ and 100 °C. The affinity for TBA in the outward-facing states is also about 50 times higher than in the inward-facing (Fig. 6). The decreased affinities at elevated temperatures are mostly due to the progressively less favorable free energy of Na^+ binding. In fact, the extrapolations suggest that the transporter does not bind the ions without substrate at all, at least in the absence of the electric field. Approximately an order of magnitude higher K_m values and two orders of magnitude higher inhibition constants in the inward facing state have been also measured for glutamate and DL-TBOA, respectively, in a mammalian homologue²⁶. Lower intracellular affinity for the substrate in both the mammalian and archaeal transporters may reflect an evolutionary conserved mechanism to optimize the efficiency of substrate transport into the cytoplasm.

Discussion

Here, we have shown that binding of Asp to Gltp_h is strictly coupled to binding of all 3 co-transported Na^+ ions and that all Na^+ ions are bound before trans-membrane movement of the transport domain takes place. Hence, Na^+ ions facilitate transport by driving substrate binding and unbinding on the opposite sides of the membrane, and not by, for example, binding to a translocation intermediate. Furthermore, while Asp does not bind to the transporter with a measurable affinity in the absence of Na^+ , 2 Na^+ ions do bind alone, albeit weakly. Similarly, the mammalian glutamate transporters bind 1 or 2 Na^+ ions weakly in a step that precedes binding of the substrate and the last Na^+ ion⁴². Hence, we suggest that binding of the first 2 Na^+ ions is a prerequisite for the consequent binding steps. The high cooperativity of Asp and Na^+ binding, which is allosteric in nature, suggests that binding of the first 2 Na^+ ions is associated with remodeling of the transporter core to form a competent substrate binding site, for which the ions pay large energetic penalty. Consistently, these early steps in the substrate binding reactions are associated with very large decreases of the protein heat capacity, which cannot be explained solely by the local conformational changes such as openings or closures of the gates. Instead, large C_p s suggest that the conformational changes are more extensive and/or are accompanied by rigidification of the protein or the involvement of water molecules. Consequent binding of the substrate backbone occurs with little additional conformational changes, while occlusion of the binding pocket and binding of the third Na^+ ion is again associated with large C_p s, indicative of complex processes. It is interesting that the reaction steps associated with Na^+ binding, and not with complexation of the substrate backbone, produce unexpectedly large heat capacity changes. To the best of our knowledge, the C_p s associated with ion binding to transport proteins have not been previously reported. However, large C_p s have been

observed in studies of Na⁺ binding to serine proteases and attributed to rigidification of a flexible autolysis loop³⁷. By analogy, we suggest that the large *C_{ps}* associated with Na⁺ binding to Glt_{Ph} are due to diminished protein flexibility and that the apo inward facing state is more dynamic compared to the outward facing state. We conclude that Na⁺ ions do not bind to preformed sites, but instead trigger conformational changes within the protein and may also have global effects on the dynamic properties of the transporter.

In conclusion, the ability to isolate and study key conformational states of a transporter offers means to deconstruct the complex transport cycle into simple reactions amenable to quantitative analysis. Using this approach, we show that the outward and inward facing states of Glt_{Ph} are similar in their ability to couple binding of all three Na⁺ ions to binding of the substrate. However, the molecular events underlying these coupled reactions are distinct and are more complex than expected for a simple ligand binding process accompanied by local conformational changes. Although further crystallographic studies of the apo states of Glt_{Ph} will resolve the structural re-arrangements associated with ion-coupled substrate binding, the complementary thermodynamic data highlights the importance of the ensemble properties of these dynamic molecules.

Online Methods

DNA manipulations, protein preparation, concentration determination and activity assays

Double cysteine mutations were introduced within hepta-histidine cysteine-less mutant Glt_{Ph}⁵ using QuickChange. Each protein was expressed as carboxyl terminal (His)₈ fusion and purified as described previously⁵. Briefly, isolated crude membranes from DH10α *E. coli* over-expressing the protein variants were solubilized in *n*-dodecyl-β-*D*-maltopyranoside (DDM) and applied to immobilized metal affinity resin in buffer containing in mM: 10 HEPES/KOH, 100 NaCl, 0.1 Asp and 0.4 DDM. The resin was washed in the same buffer supplemented with 40 mM imidazole, and proteins eluted in the presence of 250 mM imidazole. The (His)₈ tag was removed by thrombin digestion and proteins were further purified by size exclusion chromatography (SEC)⁵ in appropriate buffers as indicated below. Protein concentration was determined by absorbance at 280 nm. The extinction coefficient was determined by conducting quantitative amino acid analysis (Keck Biotechnology Resource Laboratory, Yale University). Glt_{Ph} L66C S300C, Glt_{Ph} K55C A364C and WT Glt_{Ph} showed similar results and the final extinction coefficient used was an average from the three proteins with a value of 57,400 M⁻¹ cm⁻¹. Importantly, this value is ~2 times higher than the value estimated from sequence (<http://web.expasy.org/protparam/>). For activity assays, Glt_{Ph} was reconstituted into liposomes composed of total polar lipid extract: egg phosphatidylcholine 3:1 (w:w) at 1:50 protein to lipid ratio as described previously⁶. The proteo-liposomes were loaded with 20 mM HEPES/Tris, pH 7.4, 300 mM choline chloride and the uptake was measured at 30 °C in buffer containing 20 mM HEPES/Tris, pH 7.4, 200 mM choline chloride, 100 mM NaCl, 0.1 μM ³H Asp and increasing concentration of TBA or DL-TBOA as described⁶.

Protein crystallization and structure determination

Prior to crystallization, Glt_{ph} L66C S300C mutant was purified by SEC in buffer containing in mM: 10 HEPES/KOH, pH 7.4, 100 NaCl, 0.1 Asp and 7 *n*-decyl- β , D -maltopyranoside. Samples were concentrated to over 5 mg/ml and cross-linked with 10-fold molar excess of HgCl₂. Cross-linked protein samples were dialyzed overnight against SEC buffer, and crystallized and cryo-protected as described previously⁵. The diffraction data were collected at 1.075 Å wavelength and cryogenic temperatures at the National Synchrotron Light Source beam line X29. Data were scaled using HKL2000⁴³ and further processed using CCP4 suite of programs⁴⁴. The initial crystallographic phases were determined in Phaser⁴⁵ using the trimeric trimerization domain and the three transport domains as independent search models. The protein model was further refined in Refmac5 with TLS⁴⁶ and the electron density maps were examined in Coot⁴⁷. Following refinement, 57.8, 39.8 and 2.4 % of the backbone dihedral angles were within core, allowed and disallowed regions of the Ramachandran plot, respectively. All structural figures were prepared using Pymol⁴⁸.

Isothermal titration calorimetry

For ITC experiments, Glt_{ph} K55C A364C and Glt_{ph} L66C S300C were cross-linked following thrombin digest. To avoid chelation of Hg²⁺ ions by imidazole, proteins were exchanged into a buffer containing in mM: 10 HEPES/KOH pH 7.4, 50 NaCl, 50 KCl and 0.4 DDM, using 15 ml filters (Amicon, Inc.) with a molecular weight cutoff of 100 kDa. Proteins were concentrated to over 5 mg/ml, incubated with 10-fold molar excess of HgCl₂, and purified by SEC using the following buffer in mM: 10 HEPES/KOH, pH 7.4, 1 NaCl, 99 KCl, and 0.4 DDM. For the binding experiments in 1 M NaCl, concentration of DDM was increased to 1 mM. WT Glt_{ph} was prepared in the same way except without buffer exchange and HgCl₂ addition. Quantitative amino acid analysis of the non-hydrolyzed protein samples showed no detectable Asp or other free amino acids in the samples, showing that this protocol generates protein completely unbound from its substrate. Protein samples diluted to 15–40 μ M in buffer supplemented with appropriate concentrations of NaCl were loaded into the reaction cell of a small volume NANO ITC (TA Instruments, Inc.). Appropriate titrant was loaded into the syringe and aliquots of 1.5 μ l were injected every 3–5 minutes at constant temperature. For the competition experiments, the syringe was loaded with 200–300 μ M Asp, 600 μ M TBA and 30 mM NaCl and the cell with 40 μ M protein, 600 μ M TBA and 30 mM NaCl. Binding isotherms were analyzed using NanoAnalyze data analysis software using the independent binding site model (TA Instruments, Inc.).

Fluorescence-based binding assays

For fluorescence-based binding assays, Glt_{ph} samples were prepared as above and diluted to final concentration of 0.5–1 μ M in the same buffer as for the ITC experiments, but using 0.2 instead of 0.4 mM DDM. The binding assays were performed at 25°C in the presence of 200 nM of RH421 dye (Invitrogen, Inc.). The fluorescence was excited and the emission detected at 532 nm and 628 nm, respectively, using a QuantaMaster 40 (Photon International Technology, Inc.). The protein solutions with dye were allowed to equilibrate under illumination for ~15 minutes until the fluorescence signal was stable. Aliquots of NaCl, Asp or TBA were added to the protein and the reaction mixtures were incubated until no

additional fluorescence signal change could be detected. Binding isotherms were analyzed with SigmaPlot 12 (Systat Software, Inc.). For each ligand addition, the fluorescence signal acquired during the last 10 seconds of equilibration was averaged. The maximum signal change was determined by addition of 1 mM aspartate to the samples at the end of each titration. The fractional fluorescence change was calculated as the difference between measured and initial fluorescence normalized by the maximum fluorescence change. Asp or TBA titrations were fitted to the quadratic binding equation to take into account substrate depletion at low K_{DS} , while Na^+ titrations were fitted to Hill equation. When using the latter, care was taken that the measured K_{DS} were at least 100-fold higher than the protein concentration used. Na^+ activities were calculated as $\text{Activity} = \gamma \times [\text{Na}^+]$, where γ is the activity coefficient calculated using Debye-Huckel equation

$$\log_{10}\gamma = \frac{A\sqrt{I}}{1+B\sqrt{I}},$$

where A and B are empirical coefficients with values 0.51 and 1.5, respectively and I is the ionic strength of the solution.

Supplementary Material

Refer to Web version on PubMed Central for supplementary material.

Acknowledgements

Rockefeller high throughput screening facility is acknowledged for the use of their ITC instrument, contributing to the ITC studies. National Institute of Health grants R01 NS064357 (O.B.) and S10 RR026970 (O.B.) are acknowledged for supporting the research and providing funding for ITC instrumentation, respectively. National Synchrotron Light Source X29 beam line was used for data collection and we thank the staff for help and continuous support. We thank H. J. Appel for his advice on the use RH421 dye. We also thank Alessio Accardi for critical reading of the manuscript.

References

1. Forrest LR, Kramer R, Ziegler C. The structural basis of secondary active transport mechanisms. *Biochim Biophys Acta*. 2011; 1807:167–88. [PubMed: 21029721]
2. Guan L, Kaback HR. Binding affinity of lactose permease is not altered by the H^+ electrochemical gradient. *Proc Natl Acad Sci U S A*. 2004; 101:12148–52. [PubMed: 15304639]
3. Ryan RM, Compton EL, Mindell JA. Functional characterization of a Na^+ -dependent aspartate transporter from *Pyrococcus horikoshii*. *J Biol Chem*. 2009; 284:17540–8. [PubMed: 19380583]
4. Groeneveld M, Slotboom DJ. Na^+ : aspartate coupling stoichiometry in the glutamate transporter homologue GltPh. *Biochemistry*. 2010; 49:3511–3513. [PubMed: 20349989]
5. Yernool D, Boudker O, Jin Y, Gouaux E. Structure of a glutamate transporter homologue from *Pyrococcus horikoshii*. *Nature*. 2004; 431:811–8. [PubMed: 15483603]
6. Boudker O, Ryan RM, Yernool D, Shimamoto K, Gouaux E. Coupling substrate and ion binding to extracellular gate of a sodium-dependent aspartate transporter. *Nature*. 2007; 445:387–93. [PubMed: 17230192]
7. Reyes N, Ginter C, Boudker O. Transport mechanism of a bacterial homologue of glutamate transporters. *Nature*. 2009; 462:880–5. [PubMed: 19924125]
8. Verdon G, Boudker O. Crystal structure of an asymmetric trimer of a bacterial glutamate transporter homologue. *Nat Struct Mol Biol*. 2012; 19:355–7. [PubMed: 22343718]

9. Teichman S, Qu S, Kanner BI. A conserved asparagine residue located in the binding pocket controls cation selectivity and substrate interactions in a neuronal glutamate transporter. *J Biol Chem.*
10. Huang Z, Tajkhorshid E. Identification of the third Na⁺ site and the sequence of extracellular binding events in the glutamate transporter. *Biophys J.* 99:1416–25. [PubMed: 20816053]
11. Larsson HP, et al. Evidence for a third sodium-binding site in glutamate transporters suggests an ion/substrate coupling model. *Proc Natl Acad Sci U S A.* 107:13912–7. [PubMed: 20634426]
12. Tao Z, et al. Mechanism of cation binding to the glutamate transporter EAAC1 probed with mutation of the conserved amino acid residue Thr101. *J Biol Chem.* 2010; 285:17725–33. [PubMed: 20378543]
13. Rosental N, Bendahan A, Kanner BI. Multiple consequences of mutating two conserved beta-bridge forming residues in the translocation cycle of a neuronal glutamate transporter. *J Biol Chem.* 2006; 281:27905–15. [PubMed: 16870620]
14. Holley DC, Kavanaugh MP. Interactions of alkali cations with glutamate transporters. *Philos Trans R Soc Lond B Biol Sci.* 2009; 364:155–61. [PubMed: 18977733]
15. Bastug T, et al. Position of the third Na⁺ site in the aspartate transporter GltPh and the human glutamate transporter, EAAT1. *PLoS One.* 7:e33058. [PubMed: 22427946]
16. Huang Z, Tajkhorshid E. Dynamics of the extracellular gate and ion-substrate coupling in the glutamate transporter. *Biophys J.* 2008; 95:2292–300. [PubMed: 18515371]
17. Shrivastava IH, Jiang J, Amara SG, Bahar I. Time-resolved mechanism of extracellular gate opening and substrate binding in a glutamate transporter. *J Biol Chem.* 2008; 283:28680–90. [PubMed: 18678877]
18. Focke PJ, Moenne-Loccoz P, Larsson HP. Opposite movement of the external gate of a glutamate transporter homolog upon binding cotransported sodium compared with substrate. *J Neurosci.* 2011; 31:6255–62. [PubMed: 21508248]
19. Habeck M, Cirri E, Katz A, Karlsh SJ, Apell HJ. Investigation of electrogenic partial reactions in detergent-solubilized Na,K-ATPase. *Biochemistry.* 2009; 48:9147–55. [PubMed: 19708718]
20. Pedersen M, et al. Detection of charge movements in ion pumps by a family of styryl dyes. *J Membr Biol.* 2002; 185:221–36. [PubMed: 11891580]
21. Clarke RJ, Zouni A, Holzwarth JF. Voltage sensitivity of the fluorescent probe RH421 in a model membrane system. *Biophys J.* 1995; 68:1406–15. [PubMed: 7787026]
22. Weyand S, et al. Structure and molecular mechanism of a nucleobase-cation-symport-1 family transporter. *Science.* 2008; 322:709–13. [PubMed: 18927357]
23. Zerangue N, Kavanaugh MP. Flux coupling in a neuronal glutamate transporter. *Nature.* 1996; 383:634–7. [PubMed: 8857541]
24. Levy LM, Warr O, Attwell D. Stoichiometry of the glial glutamate transporter GLT-1 expressed inducibly in a Chinese hamster ovary cell line selected for low endogenous Na⁺-dependent glutamate uptake. *J Neurosci.* 1998; 18:9620–8. [PubMed: 9822723]
25. Owe SG, Marcaggi P, Attwell D. The ionic stoichiometry of the GLAST glutamate transporter in salamander retinal glia. *J Physiol.* 2006; 577:591–9. [PubMed: 17008380]
26. Zhang Z, et al. Transport direction determines the kinetics of substrate transport by the glutamate transporter EAAC1. *Proc Natl Acad Sci U S A.* 2007; 104:18025–30. [PubMed: 17991780]
27. Mavencamp TL, Rhoderick JF, Bridges RJ, Esslinger CS. Synthesis and preliminary pharmacological evaluation of novel derivatives of L-beta-threo-benzylaspartate as inhibitors of the neuronal glutamate transporter EAAT3. *Bioorg Med Chem.* 2008; 16:7740–8. [PubMed: 18650095]
28. Shimamoto K, et al. DL-threo-beta-benzyloxyaspartate, a potent blocker of excitatory amino acid transporters. *Mol Pharmacol.* 1998; 53:195–201. [PubMed: 9463476]
29. Shimamoto K, et al. Syntheses of optically pure beta-hydroxyaspartate derivatives as glutamate transporter blockers. *Bioorg Med Chem Lett.* 2000; 10:2407–10. [PubMed: 11078189]
30. Gomez J, Hilser VJ, Xie D, Freire E. The heat capacity of proteins. *Proteins.* 1995; 22:404–12. [PubMed: 7479713]

31. Robertson AD, Murphy KP. Protein Structure and the Energetics of Protein Stability. *Chem Rev.* 1997; 97:1251–1268. [PubMed: 11851450]
32. Loladze VV, Ermolenko DN, Makhatadze GI. Heat capacity changes upon burial of polar and nonpolar groups in proteins. *Protein Sci.* 2001; 10:1343–52. [PubMed: 11420436]
33. Prabhu NV, Sharp KA. Heat capacity in proteins. *Annu Rev Phys Chem.* 2005; 56:521–48. [PubMed: 15796710]
34. DeChancie J, Shrivastava IH, Bahar I. The mechanism of substrate release by the aspartate transporter GltPh: insights from simulations. *Mol Biosyst.* 2011; 7:832–42. [PubMed: 21161089]
35. Bergqvist S, Williams MA, O'Brien R, Ladbury JE. Heat capacity effects of water molecules and ions at a protein-DNA interface. *J Mol Biol.* 2004; 336:829–42. [PubMed: 15095863]
36. Horn JR, Brandts JF, Murphy KP. van't Hoff and calorimetric enthalpies II: effects of linked equilibria. *Biochemistry.* 2002; 41:7501–7. [PubMed: 12044184]
37. Pozzi N, Chen R, Chen Z, Bah A, Di Cera E. Rigidification of the autolysis loop enhances Na(+) binding to thrombin. *Biophys Chem.* 2011; 159:6–13. [PubMed: 21536369]
38. Myszka DG, et al. Energetics of the HIV gp120-CD4 binding reaction. *Proc Natl Acad Sci U S A.* 2000; 97:9026–31. [PubMed: 10922058]
39. Olsson TS, Williams MA, Pitt WR, Ladbury JE. The thermodynamics of protein-ligand interaction and solvation: insights for ligand design. *J Mol Biol.* 2008; 384:1002–17. [PubMed: 18930735]
40. Feller G. Protein stability and enzyme activity at extreme biological temperatures. *J Phys Condens Matter.* 22:323101. [PubMed: 21386475]
41. Wolf-Watz M, et al. Linkage between dynamics and catalysis in a thermophilic-mesophilic enzyme pair. *Nat Struct Mol Biol.* 2004; 11:945–9. [PubMed: 15334070]
42. Watzke N, Bamberg E, Grewer C. Early intermediates in the transport cycle of the neuronal excitatory amino acid carrier EAAC1. *J Gen Physiol.* 2001; 117:547–62. [PubMed: 11382805]
43. Otwinowski Z, Minor W. Processing of X-ray diffraction data collected in oscillation mode. *Methods Enzymol.* 1997; 276:308–326.
44. The CCP4 suite: programs for protein crystallography. *Acta Crystallogr D Biol Crystallogr.* 1994; 50:760–3. [PubMed: 15299374]
45. McCoy AJ, et al. Phaser crystallographic software. *J. Appl. Cryst.* 2007; 40:658–674. [PubMed: 19461840]
46. Winn MD, Isupov MN, Murshudov GN. Use of TLS parameters to model anisotropic displacements in macromolecular refinement. *Acta Crystallogr D Biol Crystallogr.* 2001; 57:122–33. [PubMed: 11134934]
47. Emsley P, Cowtan K. Coot: model-building tools for molecular graphics. *Acta Crystallogr D Biol Crystallogr.* 2004; D60:2126–2132. [PubMed: 15572765]
48. DeLano, WL. The PyMOL Molecular Graphics System. DeLano Scientific LLC; Palo Alto, CA, USA: 2008.

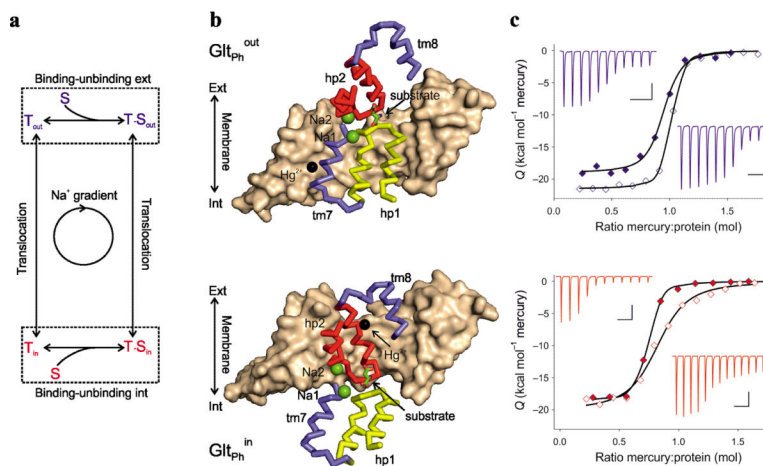


Figure 1. Constraining Glt_{Ph} in the outward and inward facing states

(a) Schematic representation of the transport cycle. The dashed boxes highlight the substrate (S) binding/unbinding equilibria on the extracellular and intracellular sides of the membrane. (b) The crystal structures of single protomers of Glt_{Ph}^{out} (top) and Glt_{Ph}ⁱⁿ (bottom) cross-linked with Hg²⁺. Trimerization domains are shown in surface representation and colored wheat. Interfacial regions of the transport domains are shown as ribbons with the remainder of the transport domain omitted for clarity. TMs 7 and 8 are colored blue, HP1 yellow and HP2 red. Bound substrates are shown as sticks and ions are emphasized as spheres with Na⁺ colored green and Hg²⁺ black. (c) ITC analysis of Hg²⁺ binding at 25 °C to Glt_{Ph} L66C S300C (top) and Glt_{Ph} K55C A364C (bottom). Shown are Hg²⁺ titrations of the apo transporters in the presence of 1 mM Na⁺ (open symbols) and Asp-bound transporters in the presence of 10 mM Na⁺ and 0.2 mM Asp (solid symbols) transporters. The black lines through the data are the best fits to the independent binding sites model with parameters listed in Supplementary Table 2. The Hg²⁺ binding thermal powers are shown in the upper (Asp-bound) and lower insets (apo) with the bar scales indicating 0.1 μcal/sec and 500 sec in vertical and horizontal directions, respectively.

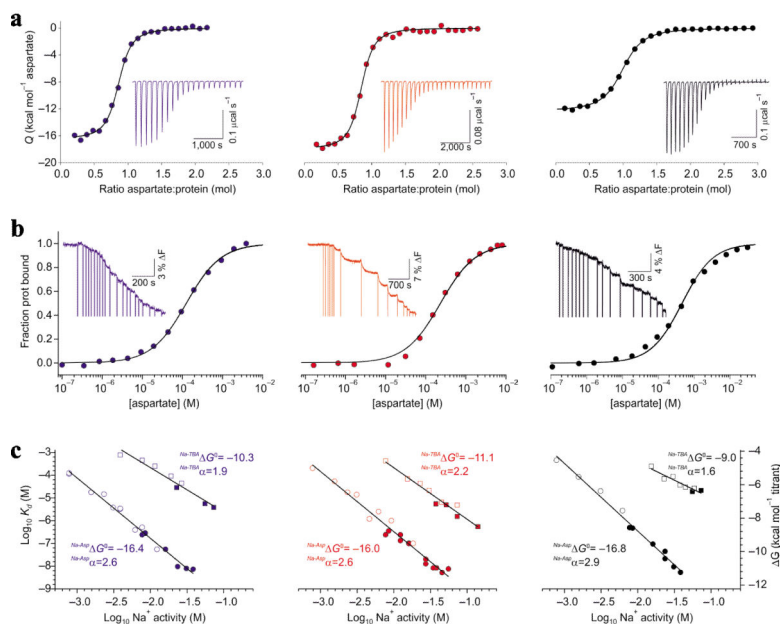


Figure 2. Na^+ -coupled binding to the outward and inward facing states

Binding data at 25 °C for $\text{Glt}_{\text{Ph}}^{\text{out}}$, $\text{Glt}_{\text{Ph}}^{\text{in}}$ and WT transporter are shown in blue (left), red (center) and black (right), respectively. **(a)** Asp binding isotherms derived from the ITC experiments conducted in the presence of 10 mM Na^+ . Solid black lines through the data are the fits to independent binding sites model with the following parameters for the three constructs, respectively: K_{DS} , 220, 211 and 493 nM; H_s , -16.4, -17.8, -12.3 kcal mol⁻¹; and apparent number of binding sites, n , 0.8, 0.8 and 1.0. Insets show the Asp binding thermal powers with the corresponding scales. **(b)** Asp titrations derived from fluorescence-based assays in the presence of 1 mM Na^+ at 25 C°. Solid black lines through the data are fits to the single-site quadratic equation with K_{DS} of 125, 232 and 457 μM for $\text{Glt}_{\text{Ph}}^{\text{out}}$, $\text{Glt}_{\text{Ph}}^{\text{in}}$ and WT, respectively. Insets show the percentage of the fluorescence change of RH421 dye as a function of time. The vertical lines mark additions of Asp aliquots. **(c)** Logarithmic plots of the Asp (circles) and TBA (squares) K_{DS} as functions of Na^+ activities. Data were obtained from ITC (solid symbols) and fluorescence-based (open symbols) experiments. Solid lines represent the best fits of the data to equation (1) with the parameters shown next to the graphs. The y-axis on the right shows corresponding binding free energies.

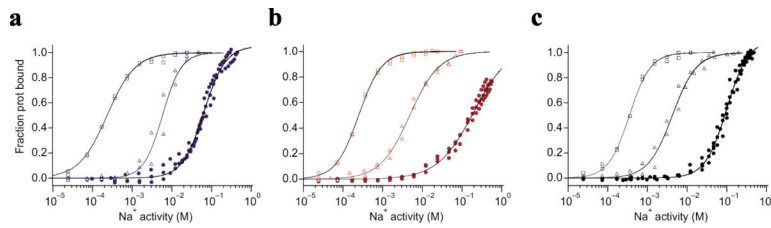


Figure 3. Na⁺ binding

Na⁺ binding isotherms at 25 °C derived from the fluorescence-based assays using RH421 dye for (a) Glt_{Ph}^{out}, (b) Glt_{Ph}ⁱⁿ and (c) WT in the absence of other ligands (solid circles), and in the presence of 1 mM Asp (open squares) or 1 mM TBA (open triangles). Solid black lines are fits to Hill equations. The fitted K_D values in mM and Hill coefficients were, respectively, in (a): 64.2, 1.6 (no Asp); 0.2, 1.2 (1 mM Asp); 5.8, 1.8 (1 mM TBA); listed in the same order in (b): 198.0, 0.9; 0.2, 1.5; 4.8, 1.2; and in (c): 99.3, 1.6; 0.4, 1.6; 4.3, 1.4. The normalization points for the fits of the data in solid circle were obtained by adding 1 mM Asp to the cuvette after the Na⁺ titrations to ensure saturation of the Na⁺ binding sites.

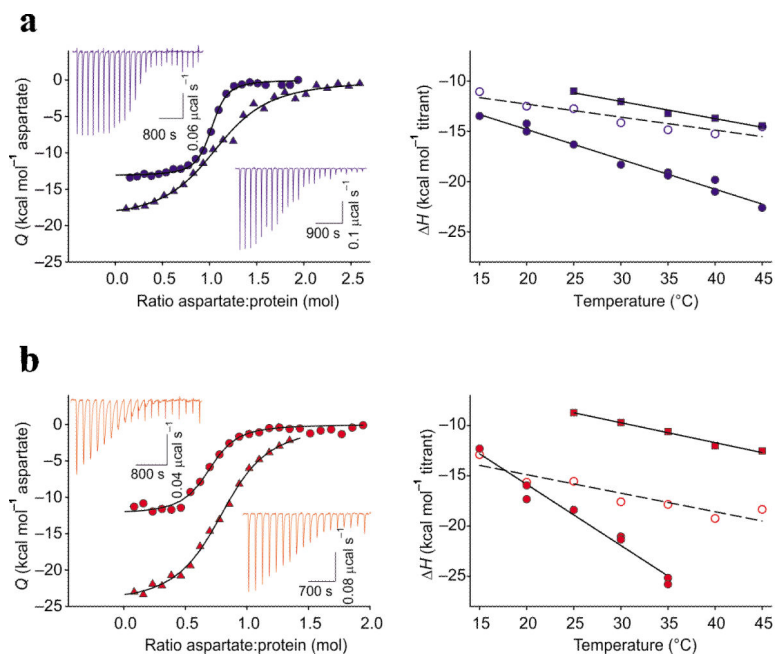


Figure 4. Binding heat capacity changes

Binding isotherms and enthalpies derived from ITC for (a) Glt_{Ph}^{out} and (b) Glt_{Ph}ⁱⁿ. Left panels, thermal powers and heats measured at 15 (solid circles and upper insets, respectively) and 35 °C (solid triangles and lower insets, respectively) are shown. The solid lines are the best fits to independent binding sites model. The fitted H in kcal/mol, K_D values in nM and n values were, respectively, in (a): -13.5 , 154 , 1.0 at 15 °C and -19.4 , 1278 and 1.1 at 35 °C; and (b): -12.3 , 373 , 0.7 at 15 °C and -25.2 , 540 and 0.8 at 35 °C. Right panels, temperature dependencies of the binding enthalpies for Asp in the presence of: 10 mM Na⁺ (solid circles), 1 M Na⁺ (open circles), and 30 mM Na⁺, 0.6 mM TBA (solid squares). The data were fitted to straight lines with the slopes corresponding to the C_{ps} of binding: -297 , -131 , -171 cal mol⁻¹ K⁻¹, respectively, for Glt_{Ph}^{out} and -608 , -184 , -198 cal mol⁻¹ K⁻¹, respectively, for Glt_{Ph}ⁱⁿ.

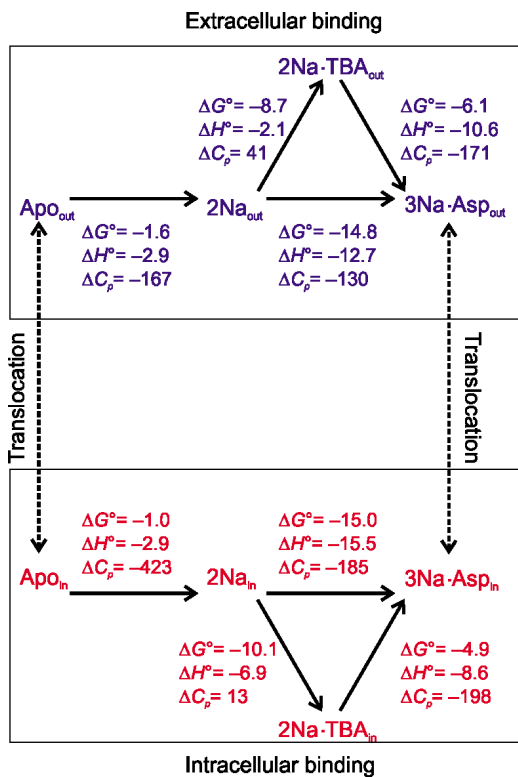


Figure 5. The thermodynamic scheme of the transport cycle and binding

Top and bottom show the thermodynamic schemes of Na^+ , Asp and TBA binding reactions with corresponding thermodynamic parameters for the outward and inward facing states, respectively. The signs of the parameters correspond to the direction of the reactions indicated by the arrowheads. The broken lines represent the isomerization reactions between the outward and inward facing states. The H° s, G° s the C_p s were either obtained experimentally or calculated as described in Supplementary Figure 6. The units are kcal mol^{-1} for H° s and G° s, and $\text{cal mol}^{-1} \text{K}^{-1}$ for C_p s.

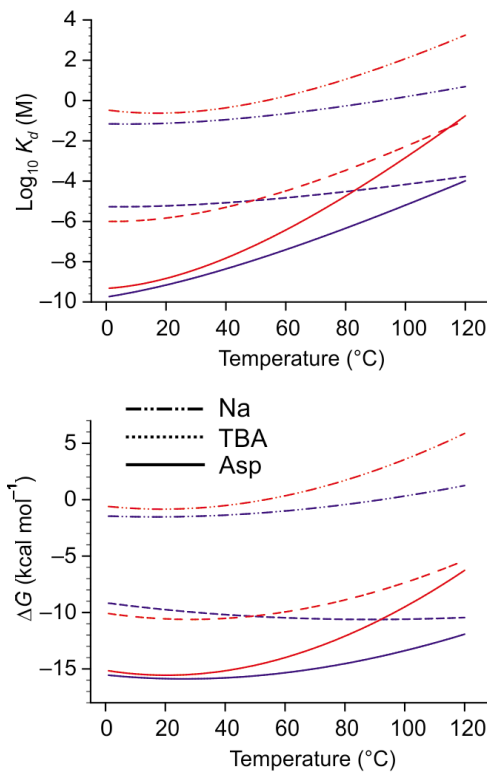


Figure 6. Temperature dependence of the binding energies

Shown are the temperature extrapolations of the binding free energies (top) and dissociation constants (bottom) for the outward (blue) and inward (red) facing states. Shown are the extrapolations for binding of 3 Na⁺/Asp (solid lines) and 2 Na⁺/TBA (broken lines) and for Na⁺ (dotted line). The K_{DS} for binding of Asp and TBA were calculated at 100 mM Na⁺.

Table 1

Data collection and refinement statistics

	$\text{Glt}_{\text{Pr}}^{\text{in}}$
Data collection	
Space group	P61
Cell dimensions	
a, c (Å)	119.7, 333.7
α, β, γ (°)	90.0, 90.0, 120.0
Resolution (Å)	50.0–4.5 (4.58–4.50)*
R_{sym} or R_{merge}	9.7 (NA)
$I / \sigma I$	14.4 (2.3)
Completeness (%)	100 (100)
Redundancy	12.6 (12.7)
Refinement	
Resolution (Å)	30 – 4.5
No. reflections	15,950
$R_{\text{work}} / R_{\text{free}}$	26.8/29.9
No. atoms	
Protein	8,694
Ligand/ion	33
Water	0
B -factors	
Protein	227.7
Ligand/ion	215.3
r.m.s. deviations	
Bond lengths (Å)	0.004
Bond angles (°)	0.8

* Values in parentheses are for highest-resolution shell.

Author Manuscript

Author Manuscript

Author Manuscript

Author Manuscript